Preprints (www.preprints.org) | NOT PEER-REVIEWED | Posted: 18 March 2022 doi:10.20944/preprints202203.0259.v1

Article

In Vivo Renal Lipid Quantification by Accelerated Magnetic Resonance Spectroscopic Imaging at 3 T: Feasibility and Reliability Study

Ahmad A. Alhulail [1,*], Mahsa Servati [2,3], Nathan Ooms [2,3], Oguz Akin [4], Alp Dincer [5,6], M. Albert Thomas [7], Ulrike Dydak [2,3], and Uzay E Emir [2,8,*]

1 Department of Radiology and Medical Imaging, Prince Sattam bin Abdulaziz University, Al Kharj, Saudi Arabia; a.alhulail@psau.edu.sa
2 School of Health Sciences, Purdue University, West Lafayette, Indiana, USA; mservati@purdue.edu (M.S.); naooms@purdue.edu (N.O.); udydak@purdue.edu (U.D.); uemir@purdue.edu (U.E.E.)
3 Department of Radiology and Imaging Sciences, Indiana University School of Medicine, Indianapolis, Indiana, USA
4 Department of Radiology, Memorial Sloan Kettering Cancer Center, New York, NY, USA; akino@MSKCC.ORG (O.A.)
5 Department of Radiology, School of Medicine, Acıbadem Mehmet Ali Aydinlar University, Istanbul, Turkey; adincer@acibadem.com (A.D.)
6 Center for Neuroradiological Applications and Research, Acıbadem Mehmet Ali Aydinlar University, Istanbul, Turkey
7 Department of Radiology, University of California Los Angeles, Los Angeles, CA, USA; AThomas@mednet.ucla.edu (M.A.T.)
8 Weldon School of Biomedical Engineering, Purdue University, West Lafayette, IN, USA
* Correspondence: a.alhulail@psau.edu.sa (A.A.A.); uemir@purdue.edu (U.E.E.)

Abstract: A reliable and practical renal-lipid quantification and imaging method is needed. Here, the feasibility of an accelerated MRSI method to map renal fat fractions (FF) at 3T and its repeatability were investigated. A 2D density-weighted concentric-ring-trajectory MRSI was used to accelerate acquiring 48×48 voxels (each of 0.25 ml spatial-resolution) without respiratory navigation implementations. The data was collected over 512 complex-FID timepoints with a 1250 Hz spectral bandwidth. The MRSI sequence was designed with a metabolite-cycling technique for lipid-water separation. The in vivo repeatability performance of the sequence was assessed by conducting a test-reposition-retest study within healthy subjects. The coefficient of variation (CV) in the estimated FF from the test-retest measurements showed a high degree of repeatability of the MRSI-FF (CV= 4.3 ±2.5%). Additionally, the matching level of spectral signature within the same anatomical region was also investigated, and their intrasubject repeatability was also high, with a small standard deviation (8.1 ±6.4%). The MRSI acquisition duration was ~3 minutes only. The proposed MRSI technique can be a reliable technique to quantify and map renal metabolites within a clinically acceptable scan time at 3T that supports the future application of this technique for the non-invasive characterization of heterogeneous renal diseases and tumors.

Keywords: kidney; renal; lipid; fast MRSI

1. Introduction

The accumulation of lipids within and around kidney tissues has been linked to different renal pathophysiologies [1–4]. Recently it was suggested that fatty kidney disease deserves designation as a specific clinical entity similar to fatty liver disease [5]. With this increase of interest in renal lipids, a non-invasive in vivo method to investigate their accumulation levels and locations is needed. Proton magnetic resonance imaging (MRI) and spectroscopy (MRS) methods have shown their potential to assess lipid-related kidney diseases, such as diabetic nephropathy, using fat fraction (FF) quantification [6–9].

© 2022 by the author(s). Distributed under a Creative Commons CC BY license.

Preprints (www.preprints.org) | NOT PEER-REVIEWED | Posted: 18 March 2022 doi:10.20944/preprints202203.0259.v1

Different MRI technique for detecting abdominal lipid has been introduced [10–14]. However, these imaging methods provide the summed fat fraction information, as they cannot differentiate the lipid components (triglyceride fatty acids). Alternatively, indirect detection of intracellular lipid (since it is considered a biomarker of renal cell carcinoma (RCC)) has been previously tried by an MRI method based on the signal drop in out-of-phase T1-weighted images [15–17]. This limitation of MRI can be addressed by implementing MRS, which can directly identify specific fatty acids and other metabolites like choline and lactate that can be used to help in differentiating and grading RCC [18–23]. Due to the alteration in lipid content within the tumor cells of RCC, differentiation from other histological subtypes could be feasible by detecting intracellular lipid contents. This suggests that MRS could be useful for RCC characterization and tumor grading. However, renal MRS remains technically challenging. Although single-voxel MRS can differentiate these lipid peaks in the kidney, it does not provide the lipid peak distributions within large heterogeneous tumors. Conventional magnetic resonance spectroscopic imaging (MRSI) addresses this limitation by delivering spatially resolved spectra over many voxels, but requiring a long acquisition time [24–26].

We recently demonstrated a high-resolution, density-weighted concentric ring trajectory (DW-CRT) metabolite cycling (MC) free induction decay (FID) MRSI acquisition technique to provide the spatially resolved musculoskeletal water and lipid spectra simultaneously [27]. In this work, our major goal was to investigate the feasibility of this accelerated MRSI acquisition to acquire reliable quantitative renal data in healthy volunteers with the intent to establish the signature of the lipid composition of healthy renal tissues, which will be used as a future tool for non-invasive characterization of renal diseases.

2. Results

The MRSI data that was collected in 3 minutes and 16 seconds was used to calculate FF maps. Examples of these MRSI FF maps are shown in Figure 1, where they were overlaid over their corresponding structural MRI images.

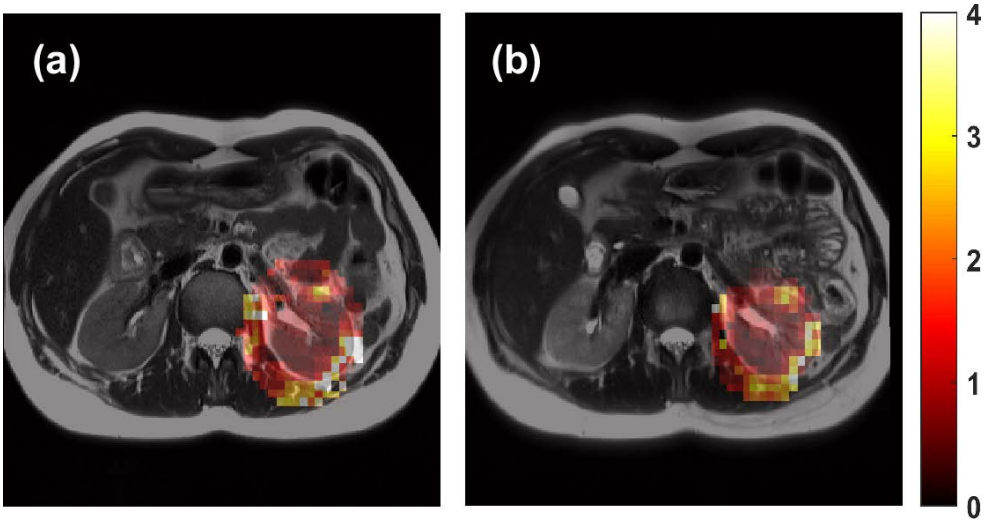

Figure 1. Representative data from: (a) the baseline; and (b) repeated scans. The kidney hilum was used as an anatomical marker to acquire the data from the same axial slice. The color-coded area is the coregistered MRSI fat-fraction map (masked about the left kidney) overlaid over its corresponding structural MRI image.

The MRSI renal fat quantification per subject and the repeatability results were summarized in Table 1. The calculated mean CV was 4.3 ± 2.5%, representing excellent repeatability.

Preprints (www.preprints.org) | NOT PEER-REVIEWED | Posted: 18 March 2022 doi:10.20944/preprints202203.0259.v1

Table 1. Fat quantification and its repeatability results.

Subject	Mean FF [%]	CV [%]
1	1.01 ± 0.05	4.90
2	1.60 ± 0.02	1.30
3	1.11 ± 0.06	5.80
4	1.69 ± 0.03	2.00
5	2.00 ± 0.15	7.40

FF, Fat-fraction; CV, Coefficient of variation.

As shown in Figure 2, the comparison between the spectral signature from the repeated scans within the same anatomical region (kidney-cortex) showed a high consistency between the scans with high intrasubject repeatability of spectral signature (CV = 8.1 ± 6.4%).

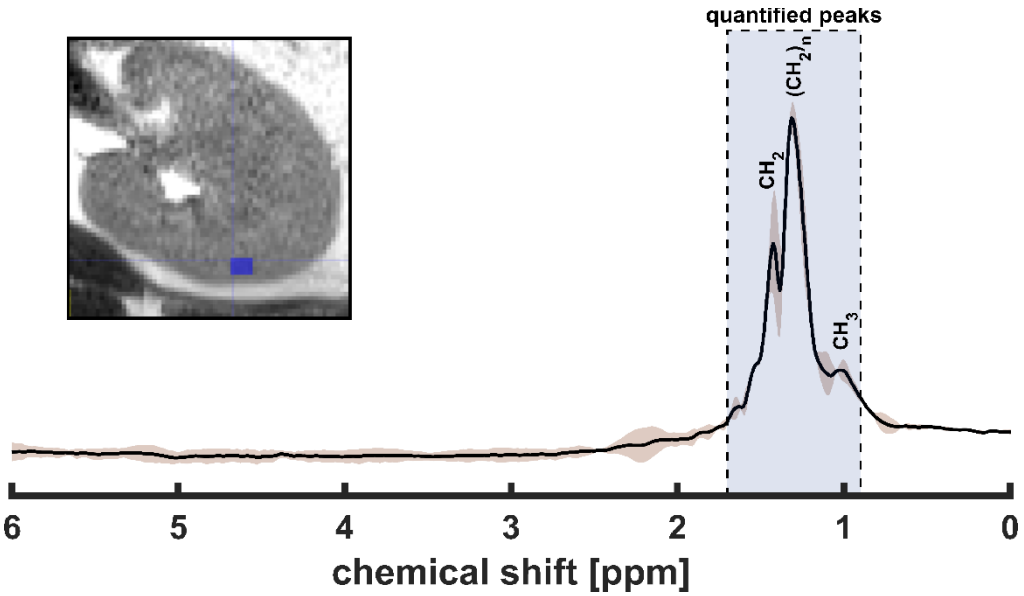

Figure 2. The spectral signature from the repeated scans within the kidney cortex. The image on the corner shows the region of interest (dark blue box) where the spectra were evaluated. The solid black line represents the mean signal, and the brown shade represents the standard deviation of the test-retest signal acquired from the same anatomical region. The blue shade highlights the peaks bandwidth that has been covered to quantify the fat fraction. The labeled lipid peaks represent fatty acids of different saturation [CH_3 at 0.9 ppm, $(CH_2)n$ at 1.3 ppm, and CH_2 around 1.6 ppm].

The structural images produced by MRSI also provided general anatomical features comparable to the MRI structural images, but with fewer details (Figure 3).

Preprints (www.preprints.org) | NOT PEER-REVIEWED | Posted: 18 March 2022 doi:10.20944/preprints202203.0259.v1

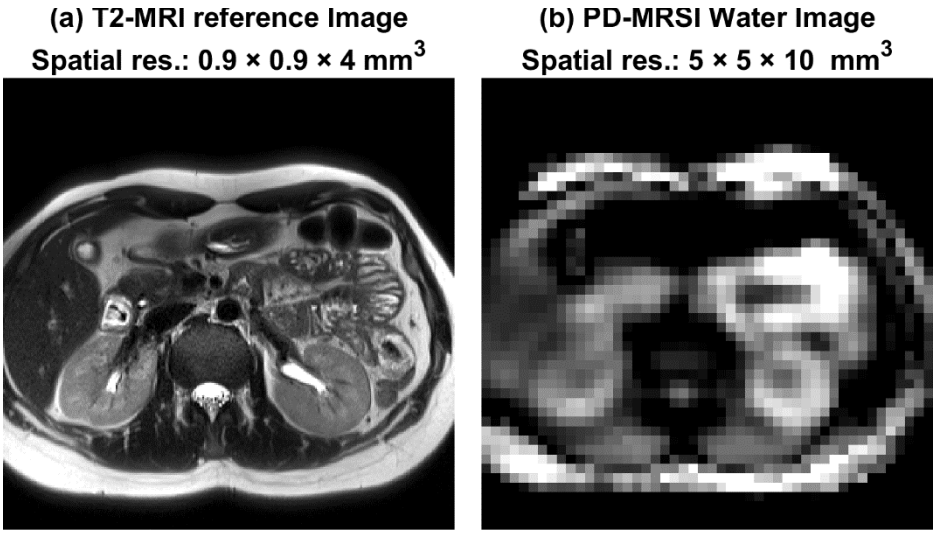

Figure 3. Example of the anatomical image outputs. (a) a T2-MRI anatomical image (0.9 × 0.9 × 4 mm^3); and (b) is the PD-water-only-MRSI anatomical image (5 × 5 × 10 mm^3) for the same subject. Although spatial resolution and contrast are different (due to the variation in sequence parameters), similar structural details of the anatomy were demonstrated by both sequences.

3. Discussion

In this work, our accelerated MRSI technique was evaluated for assessing the renal fat content at clinically available magnetic strength (3 T). The MRSI method showed promising results. High reliability of fat-fraction quantifying (CV <5%) and good imaging abilities (anatomical representation) were demonstrated. The signature of lipid spectra from the same kidney region was also consistent between the scan sessions. The MRSI data acquisition was completed within about 3 minutes, which is relatively short compared to most common MRSI techniques.

Although the MRSI was acquired without the respiratory gating, the image and quantitative data were of good quality. Scanning without respiratory gating helped to maintain a short acquisition time. The main factor contributing to achieving good results without respiratory gating is how the data were collected and post-processed. Each data set was composed of in-phase and out-of-phase spectra. The prominent water peaks within these spectra were matched to compensate for the potential motions. However, this will need a good shimming to reduce the peak width that eventually improving the water-peak matching process. In this work, the average of the measured spectral linewidth was 24.5 ± 0.4 Hz, which was enough to achieve good outcomes. Although the technique provided a high degree of reproducibility of fat fraction, it would be interesting to acquire additional data set with a respiratory gating method and compare their results in the future. The improving effect of breath-hold on the spectral quality of visible metabolites has been investigated in a previous MRS study [28]. In this previous MRS study, the SNRs of the peaks of lipids and trimethylamine (TMA) moiety of choline metabolites were improved with Breath-hold, as less contamination from surrounding tissue occurred. It is worth mentioning that this improvement has been noticed in a large single voxel (8 ml), which suffers more contamination if compared with the smaller voxels (0.25 ml) that were used in our method. In the same study, to employ the breath-holding approach with multivoxel spectroscopy, they suggested filling the k-space in segments to allow the patient to re-breathe. Although this segmentation of acquisition can allow a breath-holding approach, it prolongs the scan session duration. Thus, the implemented post-processing self-motion correction and smaller voxel sizes can promote our proposed method as a good alternative to improve the data quality and reduce the scan time.

The MRSI images provided structural information that is sufficient to determine the anatomical landmarks. For instance, as shown in Figure 3, one can identify kidneys and

Preprints (www.preprints.org) | NOT PEER-REVIEWED | Posted: 18 March 2022 doi:10.20944/preprints202203.0259.v1

liver within the MRSI, which is in good agreement with its corresponding MRI image. However, anatomical detail is not as good as what could be obtained with dedicated MRI sequences due to the lower MRSI spatial resolution, which is a standard limitation of most available MRSI sequences.

The exact MRSI sequence was previously tested on muscles and provided high-quality quantification results [27]. Here, we tested it on a more challenging area (moving and heterogeneous). In addition to extending the practicality of the sequence by granting more applications through the body regions, we decided to evaluate the technique on the kidney because of the clear need. According to the published reports in the field, there is some heterogeneity among studies regarding the mechanisms, consequences, and localization of renal lipid accumulation in the kidney, with a few in vivo studies performed on humans [1]. Additionally, the importance of metabolic imaging as a potential biomarker and research aid has been expressed in earlier publications [2]. Moreover, a need for a reliable MR spectroscopy method to quantify triglycerides in kidney structures was also expressed within other studies [29]. Although single-voxel MRS showed its powerful ability to provide unique information that can help diagnose many health disorders, it still faces several challenges. Some of the limitations of renal-MRS include its relatively low spatial resolution and the difficulty of assessing large heterogeneous tumors [18]. For instance, in addition to lipid fatty acids, MR spectroscopy methods allow gathering extra information about other metabolites such as choline, which was also used as a biomarker of RCC in the past [20]. However, the choline peak was clearer in the relatively larger tumors, which returned to the potential volume effect factor that overwhelmed the choline peak [20]. Nevertheless, the signature of metabolites in normal and RCC tissues is different between the cortex and medulla, as shown in a previous ex vivo study [30]. This anatomical difference needs a higher spatial resolution than what is used in MRS. Therefore, employing MR spectroscopy techniques that can provide the opportunity to evaluate large heterogeneous tumors and of higher spatial resolution is required. Accordingly, our proposed MRSI method can facilitate the non-invasive acquisition of human kidney data to provide a clearer idea about the renal lipid role in pathophysiology. In addition to differentiating and grading RCC tumors, another potential application of the proposed renal-MRSI can include the diabetic kidney, which has been evaluated before using the MRS approach [9].

4. Materials and Methods

4.1. Human Subjects

In vivo abdominal MRIs were performed in five healthy volunteers [four males and one female; average age 31 ± 5 years; body mass index (BMI) = 25 ± 4 kg/m^2]. The study was conducted in accordance with the institutional review board of Purdue University. Informed written consent was obtained from each volunteer prior to their scan.

4.2. Test-retest Study

To evaluate the repeatability of the kidney-MRSI method, test-retest studies were conducted. The studies were performed on a 3 Tesla Siemens Prisma scanner (Siemens Healthineers, Germany). Subjects were asked to lie on a spine coil in a head-first supine position before a flexible coil (18-channel body) was placed above their abdominal region.

The acquisition protocol included two sequences, 1) a high-resolution T2-HASTE MRI sequence to provide structural reference images, and 2) the proposed DW-CRT [31] MC FID-MRSI acquisition, which is used for fat fraction quantification [27].

The high-resolution T2-HASTE MRI reference images were acquired with TE/TR = 82/1200 msec, FA = 150°, number of averages = 1, spatial resolution = 0.9 × 0.9 × 4 mm^3, FOV = 280 x 280 mm^2, echo train length = 83.

Preprints (www.preprints.org) | NOT PEER-REVIEWED | Posted: 18 March 2022 doi:10.20944/preprints202203.0259.v1

The DW-CRT MRSI was prescribed using a Hanning-window and the following parameters: acquisition delay = 4 msec, TR = 1000 msec, FA = 90°, number of averages = 1, FOV = 240 × 240 mm^2, matrix size = 48 × 48, extractable voxel resolution = 5 × 5 × 10 mm^3 (0.25 ml nominal spatial resolution), TA = 192 sec, number of rings = 24, points-per-ring = 64, temporal samples = 512, spatial interleaves = 4, time acquire = 96 sec, and spectral bandwidth = 1250 Hz. No respiration navigation/triggering was used. This resulted in total acquisition duration of 3 minutes and 16 seconds. To enhance the static field (B_0) homogeneity, the left kidney area was shimmed before acquiring the MRSI data. The typical full width at half maximum (FWHM) was 24.5 ± 0.4 Hz.

After a 30 minutes break outside the scanner, the subject returned to the scanner table and was repositioned before the repeat scan was acquired using the same scanning protocol. For repeatability purposes, the MRSI data were obtained from an axial slice that demonstrated the same anatomy, marked by the kidney hilum (Figure 1).

4.3. MRSI Post-processing

The MRSI data were reconstructed and post-processed offline in *MATLAB* (MathWorks, Natick, MA). The gridding and the fast Fourier transform were performed using the nonuniform fast Fourier transform method [32], and without *post hoc* density compensation, as DW-CRT is already weighted by design [33]. The B_0 inhomogeneity was corrected by calculating the ΔB_0 maps described in our previous work [34]. Here, the ΔB_0 maps were calculated based on the first 2 MRSI phase-unwrapped images (TE1= 4 msec and TE2= 4.8 msec). The voxel-wise frequency and phase corrections were performed using cross-correlation and least-square fit algorithms, respectively, as described in Emir et al. [35]. The FIDs were smoothed using a Gaussian filter of 250-msec timing parameter and zero filling to 1024 time points. Next, the water-only and the metabolite-only spectra were created by summing and subtracting the alternating FIDs, respectively, as described in Alhulail et al. [27].

4.4. Fat Fraction Quantification and Mapping

To estimate the signal under each spectral peak, spectral fitting was performed using LCModel [36]. An example of fitted spectra can be found in Figure 4. The integrated signals of each fitted lipid peak (between 0.8 – 1.7 ppm) and water peak were used to calculate the percentage of FF as follows:

$$\mathrm{FF} = \frac{Lipid\ signal}{Total\ of\ lipid\ \&\ water\ signals} . 100 \quad (1)$$

To generate quantitative FF maps, the preceding process was performed for all the voxels of the left kidney.

Preprints (www.preprints.org) | NOT PEER-REVIEWED | Posted: 18 March 2022 doi:10.20944/preprints202203.0259.v1

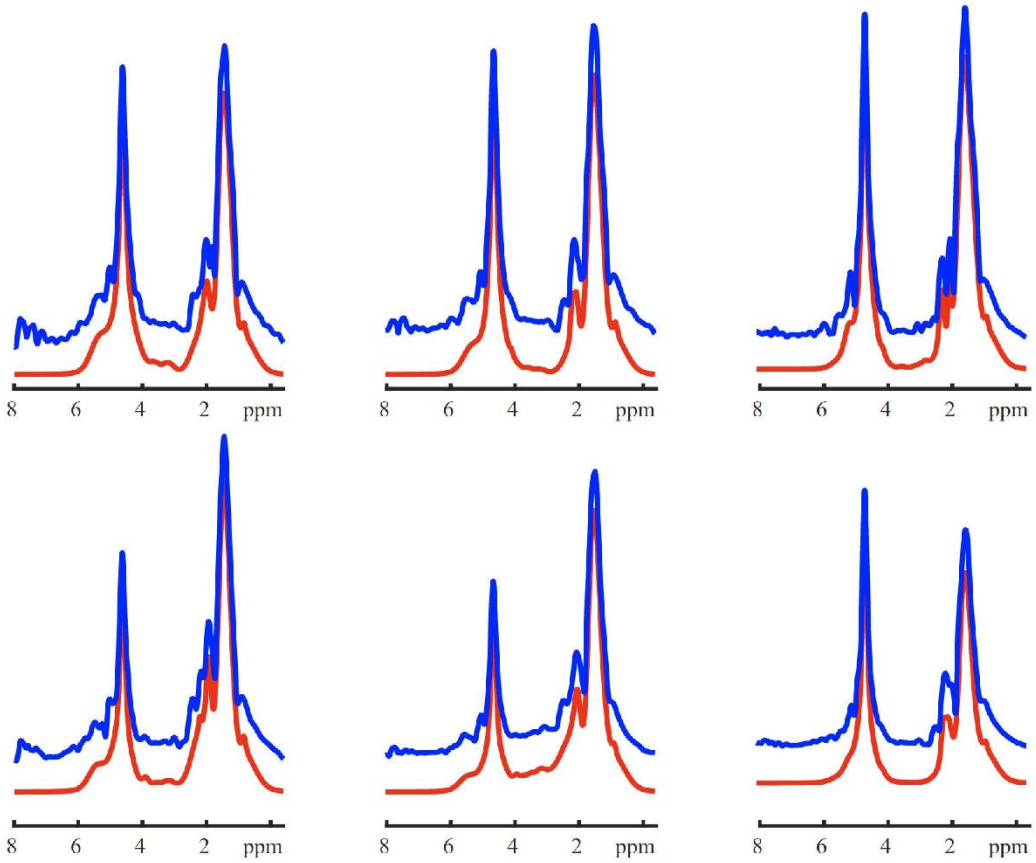

Figure 4. Example of lipid-only renal spectra fitting. Six spectra from adjacent voxels within the kidney are demonstrated. The blue lines represent the MRSI spectra, and the red lines represent their fit.

4.5. ROI Assignment and Statistical Analysis

The FF maps were first co-registered to their corresponding MRI images, which provide more precise structural details (Figure 1). Next, to assess the quantification repeatability, regions of interest (ROIs) were carefully drawn to cover several MRSI voxels only within the cortex region (to reduce anatomical variations) of the left kidney (Figure 2). Finally, the intra-subject coefficients of variation (CV) of the ROI's FF were used to evaluate the repeatability of the MRSI outcomes.

5. Conclusions

The 2D density-weighted concentric ring trajectory MRSI is a reliable non-invasive method to quantify and map renal fat fractions. In addition, it provides a promising tool to further evaluate various renal diseases, such as diabetic kidney and renal tumors with their subtypes.

Author Contributions: Conceptualization, funding acquisition, methodology, investigation, data curation, formal analysis, writing—original draft preparation, A.A. A. and U.E.E.; investigation, formal analysis, and writing—review and editing, M.S.; supervision, writing—review and editing, M.A.T. and A.D; supervision, funding acquisition, writing—review and editing, O.A. and U.D.; investigation, writing—review and editing, N.O. All authors have read and agreed to the published version of the manuscript.

Funding: This research was funded by the Indiana CTSI and grant #UL1TR001108 from the NIH, NCATS, CTS Award, and a pilot grant by the College of Health and Human Sciences in Purdue

Preprints (www.preprints.org) | NOT PEER-REVIEWED | Posted: 18 March 2022 doi:10.20944/preprints202203.0259.v1

University. Oguz Akin, MD was funded in part through the NIH/NCI Cancer Center Support Grant P30 CA008748.

Institutional Review Board Statement: The study was conducted in accordance with the guidelines of the institutional review board of Purdue University (protocol code 1102010525 on January 24, 2020).

Informed Consent Statement: Informed consent was obtained from all subjects involved in the study.

Data Availability Statement: All data, tables, and figures in this manuscript are original, and data are available on request from the corresponding authors, as it has not been uploaded to an online database.

Conflicts of Interest: The authors declare no conflict of interest.

References

1. Bobulescu, I.A. Renal lipid metabolism and lipotoxicity. *Curr Opin Nephrol Hypertens* 2010, *19*.
2. De Vries, A.P.J.; Ruggenenti, P.; Ruan, X.Z.; Praga, M.; Cruzado, J.M.; Bajema, I.M.; D'Agati, V.D.; Lamb, H.J.; Barlovic, D.P.; Hojs, R.; et al. Fatty kidney: Emerging role of ectopic lipid in obesity-related renal disease. *Lancet Diabetes Endocrinol* 2014.
3. Opazo-Ríos, L.; Mas, S.; Marín-Royo, G.; Mezzano, S.; Gómez-Guerrero, C.; Moreno, J.A.; Egido, J. Lipotoxicity and diabetic nephropathy: Novel mechanistic insights and therapeutic opportunities. *Int J Mol Sci* 2020.
4. Takahashi, T.; Wang, F.; Quarles, C.C. Current MRI techniques for the assessment of renal disease. *Curr Opin Nephrol Hypertens* 2015.
5. Mende, C.W.; Einhorn, D. Fatty kidney disease: A new renal and endocrine clinical entity? Describing the role of the kidney in obesity, metabolic syndrome, and type 2 diabetes. *Endocr Pract* 2019.
6. Wang, Y.C.; Feng, Y.; Lu, C.Q.; Ju, S. Renal fat fraction and diffusion tensor imaging in patients with early-stage diabetic nephropathy. *Eur Radiol* **2018**, doi:10.1007/s00330-017-5298-6.
7. Notohamiprodjo, M.; Goepfert, M.; Will, S.; Lorbeer, R.; Schick, F.; Rathmann, W.; Martirosian, P.; Peters, A.; Müller-Peltzer, K.; Helck, A.; et al. Renal and renal sinus fat volumes as quantified by magnetic resonance imaging in subjects with prediabetes, diabetes, and normal glucose tolerance. *PLoS One* **2020**, doi:10.1371/journal.pone.0216635.
8. Yang, J.; Zhang, L.J.; Wang, F.; Hong, T.; Liu, Z. Molecular imaging of diabetes and diabetic complications: Beyond pancreatic β-cell targeting. *Adv Drug Deliv Rev* 2019.
9. Jonker, J.T.; De Heer, P.; Engelse, M.A.; Van Rossenberg, E.H.; Klessens, C.Q.F.; Baelde, H.J.; Bajema, I.M.; Koopmans, S.J.; Coelho, P.G.; Streefland, T.C.M.; et al. Metabolic imaging of fatty kidney in diabesity: Validation and dietary intervention. *Nephrol Dial Transplant* **2018**, doi:10.1093/ndt/gfx243.
10. Pokharel, S.S.; Macura, K.J.; Kamel, I.R.; Zaheer, A. Current MR imaging lipid detection techniques for diagnosis of lesions in the abdomen and pelvis. *Radiographics* **2013**, *33*, doi:10.1148/rg.333125068.
11. Sijens, P.E.; Edens, M.A.; Bakker, S.J.L.; Stolk, R.P. MRI-determined fat content of human liver, pancreas and kidney. *World J Gastroenterol* **2010**, doi:10.3748/wjg.v16.i16.1993.
12. Zhang, Y.; Udayakumar, D.; Cai, L.; Hu, Z.; Kapur, P.; Kho, E.Y.; Pavía-Jiménez, A.; Fulkerson, M.; de Leon, A.D.; Yuan, Q.; et al. Addressing metabolic heterogeneity in clear cell renal cell carcinoma with quantitative Dixon MRI. *JCI insight* **2017**, doi:10.1172/jci.insight.94278.
13. Rosenkrantz, A.B.; Raj, S.; Babb, J.S.; Chandarana, H. Comparison of 3D two-point Dixon and standard 2D dual-echo breath-hold sequences for detection and quantification of fat content in renal angiomyolipoma. *Eur J Radiol* **2012**, doi:10.1016/j.ejrad.2010.11.012.
14. Wu, Y.; Kwon, Y.S.; Labib, M.; Foran, D.J.; Singer, E.A. Magnetic Resonance Imaging as a Biomarker for Renal Cell Carcinoma. *Dis Markers* 2015, *2015*.
15. Moosavi, B.; Shabana, W.M.; El-Khodary, M.; Van Der Pol, C.B.; Flood, T.A.; McInnes, M.D.F.; Schieda, N. Intracellular lipid in

Preprints (www.preprints.org) | NOT PEER-REVIEWED | Posted: 18 March 2022 doi:10.20944/preprints202203.0259.v1

clear cell renal cell carcinoma tumor thrombus and metastases detected by chemical shift (in and opposed phase) MRI: Radiologic-pathologic correlation. *Acta radiol* **2016**, *57*, doi:10.1177/0284185115572207.

16. Outwater, E.K.; Bhatia, M.; Siegelman, E.S.; Burke, M.A.; Mitchell, D.G. Lipid in renal clear cell carcinoma: detection on opposed-phase gradient-echo MR images. *Radiology* **1997**, *205*, 103–107.
17. Karlo, C.A.; Donati, O.F.; Burger, I.A.; Zheng, J.; Moskowitz, C.S.; Hricak, H.; Akin, O. MR imaging of renal cortical tumours: Qualitative and quantitative chemical shift imaging parameters. *Eur Radiol* **2013**, *23*, 1738–1744, doi:10.1007/s00330-012-2758-x.
18. Pedrosa, I.; Alsop, D.C.; Rofsky, N.M. Magnetic resonance imaging as a biomarker in renal cell carcinoma. In Proceedings of the Cancer; 2009; Vol. 115.
19. Ali, H.A.; Couch, M.J.; Menezes, R.; Evans, A.J.; Finelli, A.; Jewett, M.A.; Jhaveri, K.S. Predictive value of in vivo MR spectroscopy with semilocalization by adiabatic selective refocusing in differentiating clear cell renal cell carcinoma from other subtypes. *Am J Roentgenol* **2020**, *214*, doi:10.2214/AJR.19.22023.
20. Sevcenco, S.; Krssak, M.; Javor, D.; Ponhold, L.; Kuehhas, F.E.; Fajkovic, H.; Haitel, A.; Shariat, S.F.; Baltzer, P.A. Diagnosis of renal tumors by in vivo proton magnetic resonance spectroscopy. *World J Urol* **2014**, doi:10.1007/s00345-014-1272-y.
21. Katz-Brull, R.; Rofsky, N.M.; Morrin, M.M.; Pedrosa, I.; George, D.J.; Michaelson, M.D.; Marquis, R.P.; Maril, M.; Noguera, C.; Lenkinski, R.E. Decreases in free cholesterol and fatty acid unsaturation in renal cell carcinoma demonstrated by breath-hold magnetic resonance spectroscopy. *Am J Physiol - Ren Physiol* **2005**, doi:10.1152/ajprenal.00140.2004.
22. Kim, D.Y.; Kim, K.B.; Kim, O.D.; Kim, J.K. Localized in vivo proton spectroscopy of renal cell carcinoma in human kidney. *J Korean Med Sci* **1998**, doi:10.3346/jkms.1998.13.1.49.
23. Süllentrop, F.; Hahn, J.; Moka, D. In Vitro and in vivo 1H-MR spectroscopic examination of the renal cell carcinoma. *Int J Biomed Sci* **2012**, *8*, 94–108.
24. Al-Iedani, O.; Lechner-Scott, J.; Ribbons, K.; Ramadan, S. Fast magnetic resonance spectroscopic imaging techniques in human brain-applications in multiple sclerosis. *J Biomed Sci* **2017**, *24*, 1–19.
25. Öz, G.; Alger, J.R.; Barker, P.B.; Bartha, R.; Bizzi, A.; Boesch, C.; Bolan, P.J.; Brindle, K.M.; Cudalbu, C.; Dinçer, A. Clinical proton MR spectroscopy in central nervous system disorders. *Radiology* **2014**, *270*, 658–679.
26. Vidya Shankar, R.; Chang, J.C.; Hu, H.H.; Kodibagkar, V.D. Fast data acquisition techniques in magnetic resonance spectroscopic imaging. *NMR Biomed* **2019**, *32*, e4046.
27. Alhulail, A.A.; Patterson, D.A.; Xia, P.; Zhou, X.; Lin, C.; Thomas, M.A.; Dydak, U.; Emir, U.E. Fat–water separation by fast metabolite cycling magnetic resonance spectroscopic imaging at 3 T: A method to generate separate quantitative distribution maps of musculoskeletal lipid components. *Magn Reson Med* **2020**, doi:10.1002/mrm.28228.
28. Katz-Brull, R.; Rofsky, N.M.; Lenkinski, R.E. Breathhold abdominal and thoracic proton MR spectroscopy at 3T. *Magn Reson Med* **2003**, doi:10.1002/mrm.10560.
29. Bobulescu, I.A.; Lotan, Y.; Zhang, J.; Rosenthal, T.R.; Rogers, J.T.; Adams-Huet, B.; Sakhaee, K.; Moe, O.W. Triglycerides in the human kidney cortex: Relationship with body size. *PLoS One* **2014**, doi:10.1371/journal.pone.0101285.
30. Righi, V.; Mucci, A.; Schenetti, L.; Tosi, M.R.; Grigioni, W.F.; Corti, B.; Bertaccini, A.; Franceschelli, A.; Sanguedolce, F.; Schiavina, R.; et al. Ex vivo HR-MAS magnetic resonance spectroscopy of normal and malignant human renal tissues. *Anticancer Res* **2007**.
31. Steel, A.; Chiew, M.; Jezzard, P.; Voets, N.L.; Plaha, P.; Thomas, M.A.; Stagg, C.J.; Emir, U.E. Metabolite-cycled density-weighted concentric rings k-space trajectory (DW-CRT) enables high-resolution 1 H magnetic resonance spectroscopic imaging at 3-Tesla. *Sci Rep* **2018**, doi:10.1038/s41598-018-26096-y.
32. Fessler, J.A.; Sutton, B.P. Nonuniform fast Fourier transforms using min-max interpolation. *IEEE Trans Signal Process* **2003**, doi:10.1109/TSP.2002.807005.
33. Chiew, M.; Jiang, W.; Burns, B.; Larson, P.; Steel, A.; Jezzard, P.; Albert Thomas, M.; Emir, U.E. Density-weighted concentric rings k-space trajectory for1H magnetic resonance spectroscopic imaging at 7 T. *NMR Biomed* **2018**, doi:10.1002/nbm.3838.

Preprints (www.preprints.org) | NOT PEER-REVIEWED | Posted: 18 March 2022 doi:10.20944/preprints202203.0259.v1

34. Alhulail, A.A.; Xia, P.; Shen, X.; Nichols, M.; Volety, S.; Farley, N.; Thomas, M.A.; Nagel, A.M.; Dydak, U.; Emir, U.E. Fast in vivo 23Na imaging and T2∗ mapping using accelerated 2D-FID UTE magnetic resonance spectroscopic imaging at 3 T: Proof of concept and reliability study. *Magn Reson Med* **2021**, *85*, 1783–1794, doi:10.1002/mrm.28576.
35. Emir, U.E.; Burns, B.; Chiew, M.; Jezzard, P.; Thomas, M.A. Non-water-suppressed short-echo-time magnetic resonance spectroscopic imaging using a concentric ring k-space trajectory. *NMR Biomed* **2017**, doi:10.1002/nbm.3714.
36. Provencher, S.W. Estimation of metabolite concentrations from localized in vivo proton NMR spectra. *Magn Reson Med* **1993**, doi:10.1002/mrm.1910300604.